Environmental Technology & Innovation 37 (2025) 104061

Contents lists available at ScienceDirect

Environmental Technology & Innovation

journal homepage: www.elsevier.com/locate/eti

Binary CdS-WO_3 nanostructures supported on biochar substrate for visible-light-driven photocatalytic degradation of malachite green

Mahdi Salimi, Amin Abolghasemi Mahani *

Department of Chemical Engineering, Faculty of Engineering, Shahid Bahonar University of Kerman, Kerman, Iran

ARTICLE INFO

Keywords:
CdS
WO_3
Biochar
Photocatalytic degradation

ABSTRACT

The advancements made in the field of nanoscience have resulted in the production of semiconductor materials that are both cleaner and safer. These materials have proven to be highly effective in breaking down toxic and resistant pollutants in water. Additionally, semiconductor photocatalysts must possess ecological and environmental friendliness, which can be achieved by implementing green synthetic methods. Consequently, this research paper focuses on synthesizing biochar with a specific biomorphic structure, utilizing spent coffee grounds as a natural carbon source and bio-template. Subsequently, a nanocomposite consisting of biochar-WO_3/CdS (BC-WO_3/CdS) was successfully synthesized, and the resulting products were thoroughly characterized. Furthermore, the efficiency of synthesized nanocomposite in Malachite Green (MG) dye degradation under visible light irradiation was extensively investigated. Remarkably, a photocatalytic efficiency of approximately 98 % was achieved for MG dye with a concentration of 2 ppm, utilizing a catalyst dosage of 200 mg and maintaining a pH level of 8. In addition, the apparent reaction rate constant was obtained at 0.0548. Moreover, the materials exhibited the capability of being recycled up to 8 times without any noticeable decrease in stability.

1. Introduction

In today's era, concerns regarding water pollution have escalated due to a range of industrial, agricultural, and human-related activities (Saleh and Gupta, 2014; Ali et al., 2019; Mashkoor and Nasar, 2020; Awad et al., 2020). Among the various contaminants present in wastewater, synthetic organic dyes pose a significant threat as they are extensively used in industries such as textiles, paper, leather, food, pharmaceuticals, cosmetics, and more (Zhao et al., 2019). It is estimated that approximately 7×10^5 tonnes of various coloring chemicals, sourced from approximately 100,000 commercially available dyes, are manufactured each year (Gupta et al., 2011; Katheresan et al., 2018). The release of large volumes of dye-contaminated wastewater from various industries presents a substantial risk to the environment. Dyes have detrimental effects on human health, aquatic ecosystems, and the overall environment. The potential health risks associated with dye molecules present in wastewater are significant and include carcinogenicity, mutagenicity, and dysfunction of vital human organs, such as the liver, kidneys, brain, central nervous system, and reproductive system (Singh et al., 2018; Zhou et al., 2019). Among the dyes of concern, Malachite Green (MG) stands out as one that warrants particular attention. MG is a triarylmethane dye that finds extensive application in the global aquaculture industry as a biocide, as well as in various sectors

* Corresponding author.
E-mail address: a.m.abolghasemi@uk.ac.ir (A.A. Mahani).

https://doi.org/10.1016/j.eti.2025.104061
Received 12 October 2024; Received in revised form 19 January 2025; Accepted 25 January 2025
Available online 26 January 2025

including silk, wool, cotton, leather, paper, acrylic, food, and medical disinfectants. However, despite its widespread use, MG remains highly controversial due to its toxic properties, which have been linked to carcinogenesis, mutagenesis, teratogenicity, and respiratory toxicity (Berberidou et al., 2007). Consequently, the efficient removal of these harmful dye pollutants from wastewater, before their release into the ecosystem, not only enhances the quality of aquatic ecosystems but also brings significant economic benefits (Bulgariu et al., 2019). Consequently, there are significant concerns regarding both the environment and human health associated with this specific dye. Dye molecules typically exhibit the capacity to undergo excitation when they absorb visible light. This enables them to transfer their electrons to the conduction band of a semiconductor, as long as the excited state of the dye is suitably more negative than the conduction band of the semiconductor. This phenomenon is commonly known as dye sensitization. Utilizing this mechanism has demonstrated its effectiveness in boosting the efficiency of photocatalytic reactions employed in the degradation of dyes.

Extensive research has been conducted on tungsten trioxide (WO_3) as a highly promising photocatalyst for visible-light-driven reactions. It possesses an indirect band gap within the energy range of 2.4–2.8 eV (Miyauchi, 2008a). Additionally, WO_3 offers several advantages, including a valence band positioned at + 3.1 eV, effective absorption of solar spectrum, stable physicochemical properties, and resistance to photo-corrosion effects (Zhao and Miyauchi, 2008). Initially, pure WO_3 was considered inactive in terms of organic contaminant oxidation due to its conduction band level (+0.5 V vs. NHE) being more positive than the potential for the single-electron reduction of oxygen ($O_2/O^{2-} = -0.284$ V vs. NHE; $O_2/H_2O = -0.046$ V vs. NHE) (Torimoto et al., 2002; Miyauchi, 2008b). However, recent studies conducted by various research groups have demonstrated that the photocatalytic activity of WO_3 towards small alcohol species can be significantly enhanced by utilizing suitable cocatalysts (Arai et al., 2009; Kim et al., 2008). This enhancement is achieved through the multiple electron reduction of oxygen ($O_2/H_2O_2 = +0.68$ V vs. NHE; $O_2/H_2O = +1.23$ V vs. NHE) (Miyauchi, 2008b).

Cadmium sulfide (CdS) nanostructures have gained significant attention among the various nanostructures employed in photocatalysis. Their significant surface area, abundant adsorption sites, and strong light absorption capabilities are the primary factors contributing to this phenomenon (Liu et al., 2021). Moreover, CdS nanostructures can be readily synthesized using conventional methods such as hydrothermal (Salavati-Niasari et al., 2009), solvothermal (Zhang et al., 2007), microwave-assisted (Deng and Tian, 2013), and chemical precipitation techniques (Bao et al., 2008). Nevertheless, it is important to note that these synthesis methods often result in poor nanoparticle stability, leading to particle aggregation and subsequently reducing the photodegradation efficiency (Sanghi and Verma, 2009). Nevertheless, CdS nanostructures generally possess exceptional optical properties, making them excellent photocatalysts. As a result, they have been extensively investigated in numerous studies focusing on the photocatalytic degradation of various dyes.

In recent times, there has been growing interest in utilizing natural biowastes as precursors for the synthesis of carbon materials. This trend stems from their cost-effectiveness, renewability, and eco-friendliness. Agricultural plants have provided a diverse range of biomass materials for the production of activated carbons or mesoporous carbons. These materials include rice waste streams (Wong et al., 2018), corn stalk (Yang et al., 2018), sunflower marrow (Kang DongJuan et al. n.d), pomelo peel (Xu et al., 2017), Moringa oleifera branches (Cai et al., 2016), corncob residue (Qu et al., 2015), fungi (Zhu et al., 2011), and more. Such carbon materials are extensively utilized as electrode materials, catalyst carriers, or adsorbents. Coffee, a widely consumed beverage with an annual production exceeding five million tons, represents a significant biomass resource. The residual coffee grounds contain caffeine, tannins, and polyphenols, which can pose an environmental hazard if not properly managed (Huang et al., 2013). Given the abundant carbon content in waste coffee grounds, utilizing them as a carbon feedstock for large-scale production of high-value carbon materials holds great promise. This strategy offers the additional advantages of energy efficiency and environmental protection. Furthermore, after the boiling process, the interior small molecules precipitate out, making coffee grounds highly receptive to metal catalysts. This enhances carbon yield and leads to the development of unique pore structures.

This work lies in the development of binary CdS-WO3 nanostructures supported on a biochar substrate, which enhances photocatalytic activity under visible light for the degradation of malachite green. By utilizing biochar, derived from sustainable sources, this approach not only improves the efficiency of the photocatalytic process but also promotes the recycling of waste materials. This novel composite system offers a cost-effective and environmentally friendly solution for wastewater treatment, demonstrating significant potential for practical applications in pollutant degradation.

2. Experimental

2.1. Materials & methods

Analytical grade chemicals, including ammonium tungsten oxide monohydrate ($(NH_4)_2WO_4{\cdot}H_2O$, 99.9 %), nitric acid (HNO_3, 65 %), cadmium chloride dihydrate ($CdCl_2.2H_2O$, 98 %), and sodium sulfide (Na_2S, 98 %), were utilized in the experiment. All chemicals were procured from Sigma–Aldrich Company.

The synthesis of the BC-WO_3/CdS nanocomposite involves several steps, which are outlined below:

a) Synthesis of biochar: The coffee grounds were sourced from a local shop in Kerman, Iran. They underwent a manual cleaning process to eliminate any foreign matter and were then dried at 50°C for 24 h to remove moisture. Subsequently, the dried coffee grounds were ground using a domestic blender and sieved to obtain approximately uniform-sized particles, measuring less than 400 μm. The resulting powder was subjected to an oven temperature of 300°C for 4 hours. After cooling to ambient temperature, the powder was collected for further steps.

b) Synthesis of WO_3 nanoparticles: To synthesize these nanoparticles, the process began with dissolving 7.5 g of $(NH_4)_2WO_4{\cdot}H_2O$ in 75 mL of distilled water at a temperature of 80 °C. Once cooled, a 125 mL solution of 3.0 M nitric acid was slowly added drop by drop while stirring for 5 hours at room temperature. The resulting precipitate, which appeared yellow, was separated using a centrifuge and subsequently washed multiple times with a combination of water and ethanol. The washed precipitate was then dried at 70°C for 24 hours. In the final step, the dried precipitation was subjected to calcination in an oven at a temperature of 500 °C for 6 hours.
c) Synthesis of WO_3-CdS: In the initial stage, 0.35 g of WO_3 nanoparticles were introduced into a 60 mL of distilled water and subjected to ultrasonic treatment for 20 minutes. Subsequently, 0.89 g of $CdCl_2.2H_2O$ were incorporated into the solution and agitated at room temperature for a duration of 2 hours. Moving on to the subsequent phase, a solution comprising 0.52 g of Na_2S dissolved in 60 mL of distilled water was prepared. This solution was gradually added to the aforementioned mixture from the previous step, while continuously stirring, and the temperature was maintained at 70 °C for a period of three hours. Following this, the resulting precipitate was thoroughly rinsed three times with a combination of water and acetonitrile, and subsequently subjected to a drying process.
d) Synthesis of BC-WO_3/CdS nanocomposite: To initiate the process, 300 mg of WO_3-CdS was combined with 75 mL of distilled water, and separately, 10 mg of synthesized biochar was mixed with 75 mL of distilled water. Both mixtures were subjected to ultrasonic treatment within an ultrasonic bath for a duration of 15 minutes. Next, the WO_3-CdS solution was slowly added, drop by drop, to the biochar solution. The combined solution was then stirred for a period of 5 hours at a temperature of 60 °C. Following the stirring process, the mixture was subjected to centrifugation to separate the precipitation. The obtained precipitation was washed multiple times using a combination of water and ethanol, and subsequently dried.

2.2. Characterization studies

A Rigaku diffractometer was used to obtain the X-ray diffraction (XRD) pattern for structural characterizations. The diffractometer employed Ni-filtered CuKα radiation (λ = 1.5418 Å) and covered a diffraction angle range of 10° to 80°. The identification of functional groups present in the synthesized samples was performed using a Fourier transform infrared spectrometer (FTIR) from the Excalibur Series. The surface morphology of the BC-WO3/CdS arrays was examined using a JEOL Scanning Electron Microscope (JSM-840A, Japan). Additionally, UV-Vis spectra were acquired using a JASCO V570 UV-Vis-NIR spectrophotometer.

2.3. Method of photocatalytic degradation of malachite green paint

The investigation focused on studying the photocatalytic efficiency of a BC-WO_3/CdS nanocomposite for the decomposition of malachite green (MG) dye. To evaluate the dye's decomposition, experiments were conducted at different pH levels, ranging from 4 to 10. The initial pH of the suspensions was adjusted by employing NaOH or HCl solutions. Before subjecting the dye solutions to visible light irradiation (60-watt LED visible light bulb), they were incubated with the catalyst for 2 hours. The degradation process of the dye molecules, both in the presence and absence of nanocomposites and light, was analyzed using UV-Vis absorption spectroscopy. The results indicate that MG does not undergo degradation under visible light irradiation in the absence of a photocatalyst.

For the photocatalytic degradation of MG, visible light irradiation with a power of 60 W was utilized. The catalyst was added to a 10 mL aqueous solution of MG, and the mixture was stirred in darkness for 15 minutes to establish an absorption-desorption equilibrium between the catalyst and the dye. Subsequently, the samples were irradiated under the respective light sources. After irradiation, the solution was subjected to centrifugation and filtration to remove the dispersed catalyst particles. At each designated time interval, 3 mL of the test sample was collected, and the concentration of MG in the solution was determined using a UV-Vis spectrophotometer. The degradation efficiency was calculated using Eq. (1).

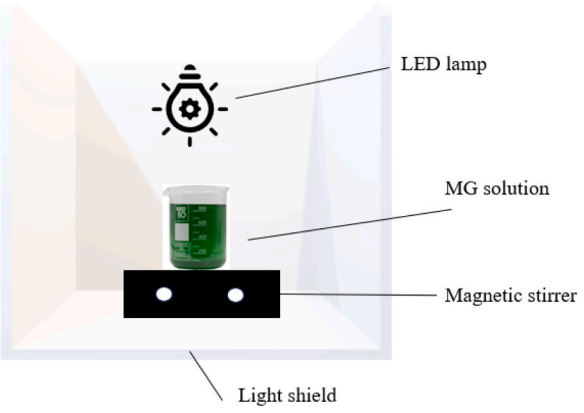

Scheme 1. A setup picture of photocatalytic experiments.

$$Degradation\ efficiency = \frac{A_0 - A_t}{A_0} \times 100 \quad (1)$$

Where A_0 represents the initial absorption maximum, while A_t represents the absorption maximum once MG has completely degraded.

3. Result

3.1. FTIR studies

To gain a more comprehensive understanding of the nanocatalyst's structure and to characterize the functional groups, the FT-IR spectra of each step involved in the nanocatalyst fabrication process were analyzed. This included (a) biochar, (b) WO_3, (c) WO_3-CdS, and (d) BS/WO_3-CdS. The results, depicted in Fig. 1, can now be described as follows:

Fig. 1a illustrates the OH stretching vibration mode, indicated by peaks present in the 3300–3500 cm^{-1} range. Additionally, the

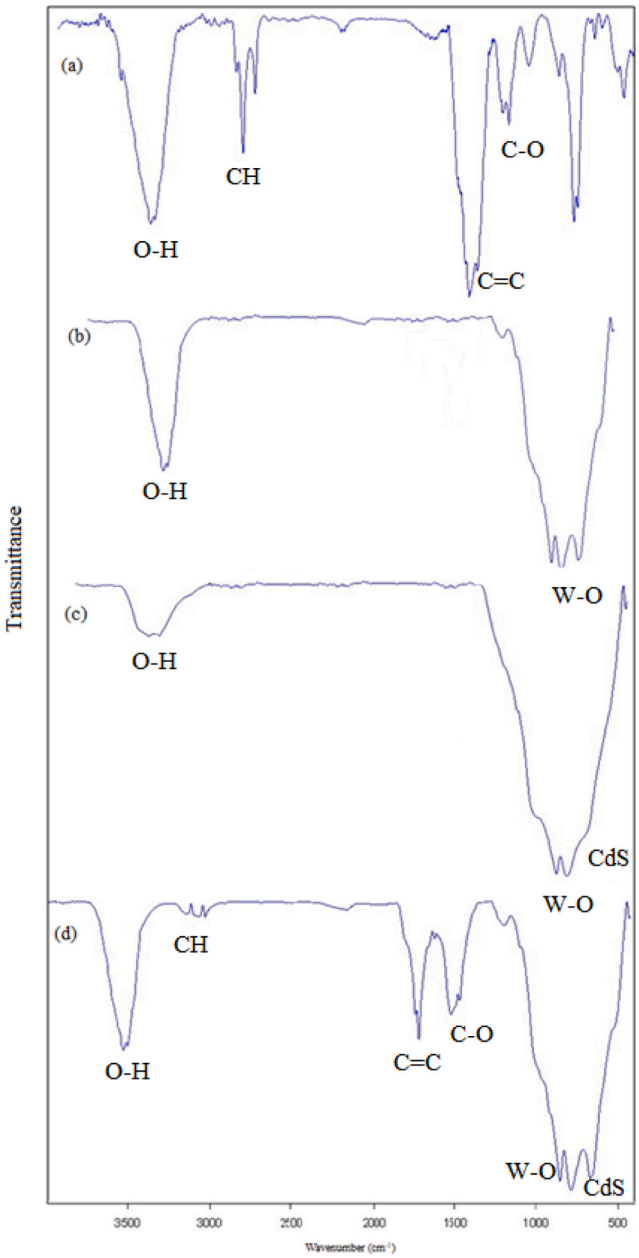

Fig. 1. FTIR spectrum of (a) biochar, (b) WO_3 nanoparticle, (c) WO_3-CdS nanostructure, and (d) BC/WO_3-CdS nanocomposite.

uptake peaks at 2851 cm^{-1} and 2920 cm^{-1} can be attributed to the stretching vibration of the C-H bond. The bonds observed at 1631 cm^{-1} and 1031 cm^{-1} signify the presence of C═C and C-O stretching vibrations, respectively. Moreover, the broad peak spanning from 700 cm^{-1} to 800 cm^{-1} corresponds to the out-of-plane C-H band. Moving on to Fig. 1b, it showcases the spectrum of WO_3 nanoparticles. Here, the peaks appearing in the regions of 639 cm^{-1} and 747 cm^{-1} are indicative of the W-O stretching vibration,

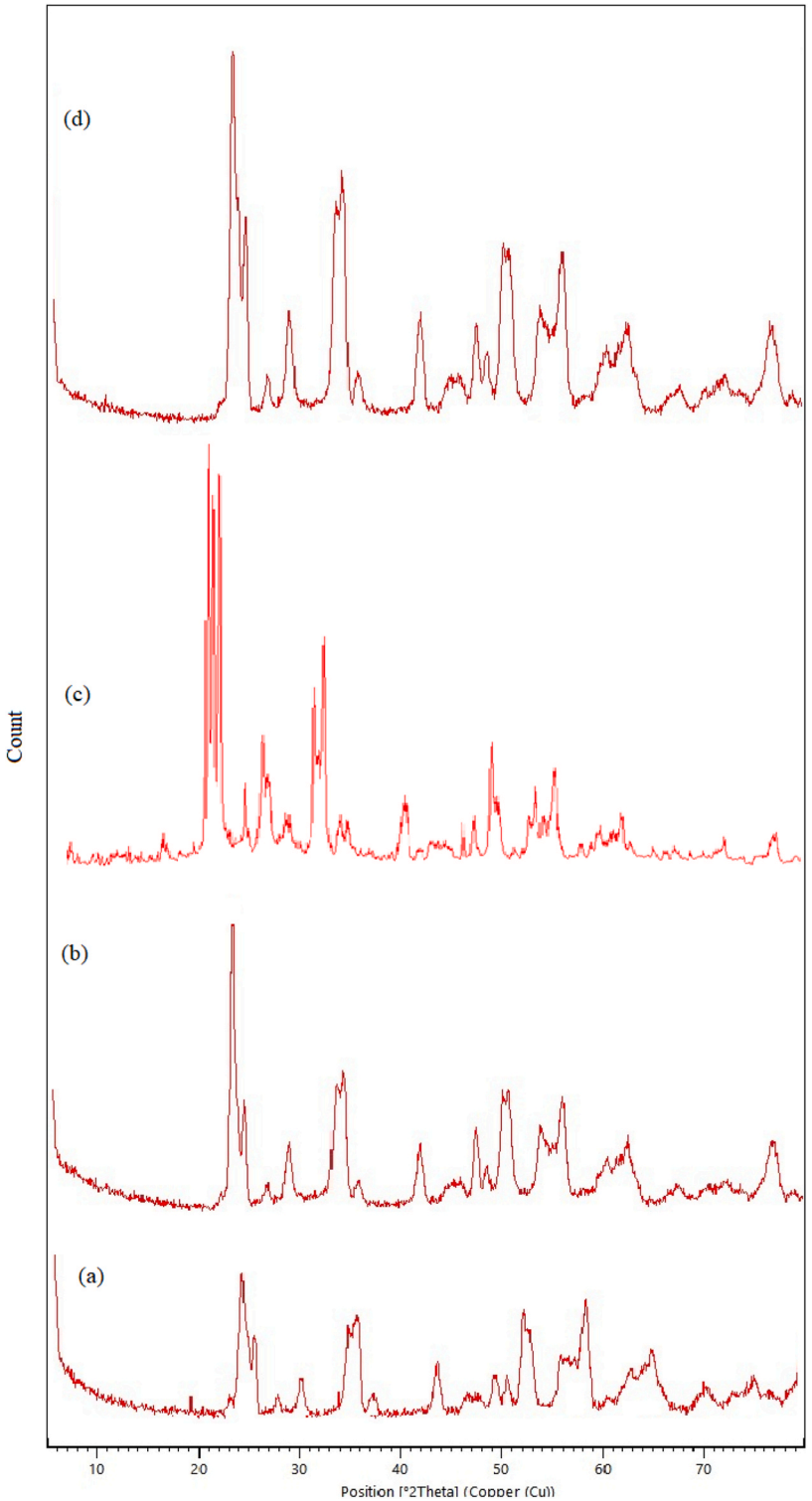

Fig. 2. XRD pattern of BC/WO_3-CdS nanocomposite.

while the peaks in the 811 cm^{-1} region suggest the W═O stretching vibration. Fig. 1c presents the FTIR spectrum for WO_3-CdS. In addition to the WO_3 carriers mentioned in the previous section, a peak associated with the Cd-S stretching vibration emerges in the 520 cm^{-1} region. Furthermore, the peak at 3422 cm^{-1} corresponds to O-H stretching vibrations, which may be attributed to water adsorption. Finally, Fig. 1d demonstrates the peak corresponding to the final nanocomposite, thereby confirming the successful synthesis of the composite.

3.2. Structural and morphological properties

To verify the crystallinity, identify the phases, and confirm the formation of WO_3, WO_3-CdS, BC/WO_3-CdS nanocomposite, and reused BC/WO_3-CdS nanocomposite, X-ray diffraction (XRD) analyses were conducted, as illustrated in Fig. 2.

In Fig. 2a, the diffraction peaks observed at angles of 23.3°, 23.8°, 24.4°, 26.8°, 35.8°, 47.6°, 50.1°, 67.8°, 74.5°, and 86.2° correspond to the (100), (002), (020), (012), (112), (200), (040), (134), (300), and (330) crystal planes of WO_3 nanoparticles, which belong to the Anorthic crystal system (Reference code: 96–101–0619).

Fig. 2b reveals additional distinct peaks, alongside those of WO_3 peaks, appearing at various angles: 26.5°, 30.7°, 44.0°, 52.1°, 54.6°, 63.9°, 70.5°, 72.6°, 80.8°, and 86.9°. These peaks are associated with the (111), (002), (022), (113), (222), (004), (133), (024), (224), and (115) crystal planes, confirming the cubic phase of the CdS nanostructure (Reference code: 96–101–1261).

In Fig. 2c, the XRD pattern of the BC/WO3-CdS nanocomposite shows, in addition to the WO_3 and CdS peaks, a notable peak at 18.5°, which is attributed to the reflection of the (101) crystal plane of the carbon-based biochar substrate.

The XRD pattern of the used nanocomposite was also analyzed. As depicted in Fig. 2d, a reduction in the intensity of some peaks or the disappearance of minor peaks suggests that certain nanoparticles may have been released after eight uses.

The composite of BC/WO_3-CdS was characterized for its surface morphology and structural features using FE-SEM and TEM. Fig. 3a depicts the spherelike structure and distribution of WO_3 and CdS nanoparticles on the surface of biochar. Notably, the image clearly illustrates the particle agglomeration on the biochar surface, which is likely attributed to the presence of nanoparticles. Furthermore,

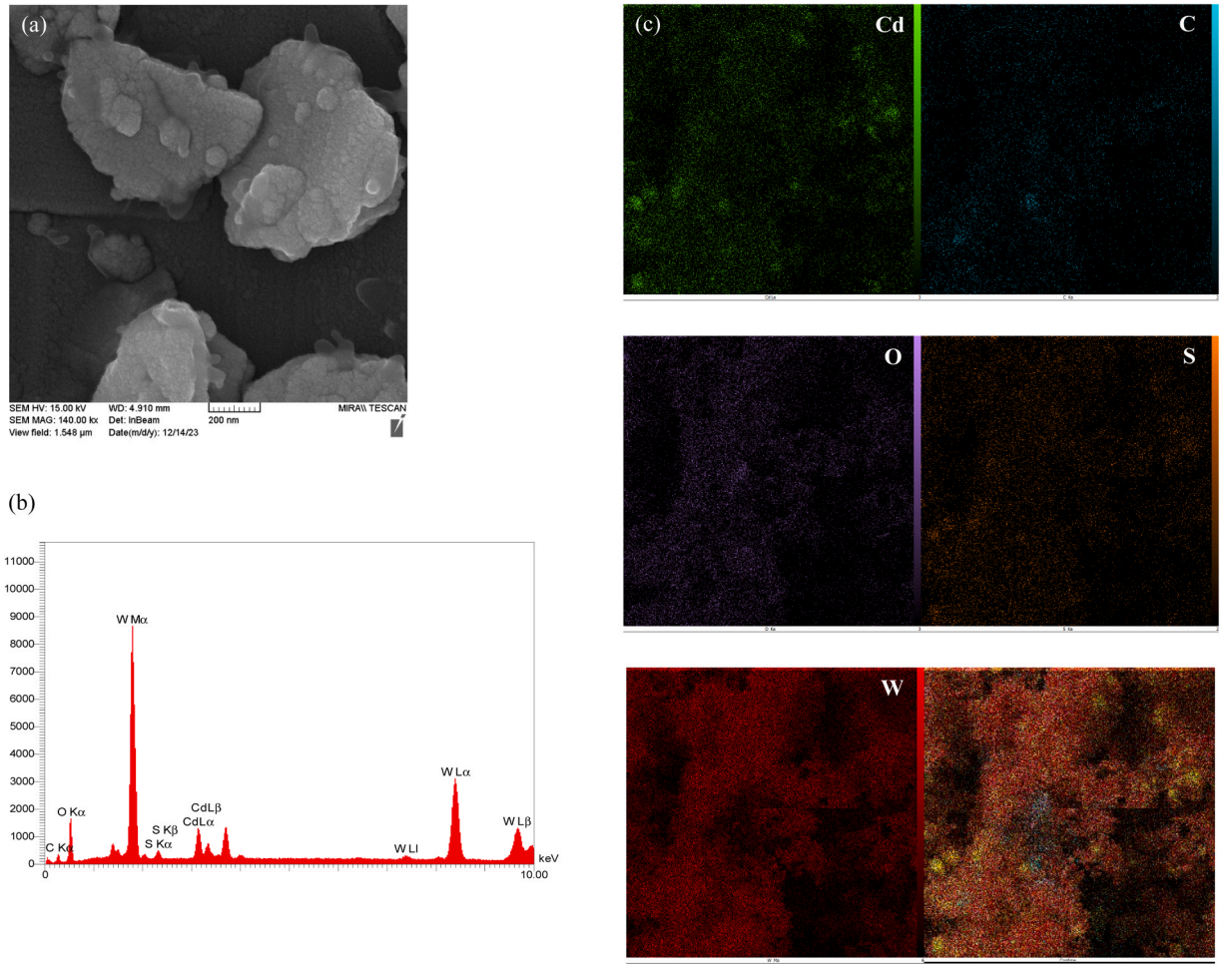

Fig. 3. FESEM (a), EDS (b), and mapping (c) of BC/WO_3-CdS nanocomposite.

EDX analysis (Fig. 3b) confirms the presence of Cd, W, S, and O elements on the surface of the biochar. Carbon is the predominant element, along with the aforementioned elements, indicating a higher abundance of biochar in the BC/WO_3-CdS composite. Additionally, the surface mapping analysis in Fig. 3c demonstrates the uniform distribution of elements on the surface of the nanocomposite.

The TEM image of the BC/WO_3-CdS nanocomposite, shown in Fig. 4, reveals the almost spherical shapes of CdS and WO_3, which are doped onto the biochar surface.

Zeta potential analysis was conducted to assess the stability and mobility of the catalyst used for the degradation of malachite green. This technique provides insights into the electrokinetic properties of the catalyst, which is crucial for understanding its behavior in suspension.

The mobility distribution presented in the analysis indicates that the majority of the catalyst particles exhibit a negative zeta potential, with a peak mobility of around -3 μm/s/cm. This negative charge suggests a stable colloidal suspension, minimizing the likelihood of agglomeration and enhancing the effectiveness of the catalyst in environmental applications.

The stability of the catalyst is particularly important in the degradation process of malachite green, a toxic dye commonly found in wastewater. A stable catalyst ensures prolonged activity and efficiency during the catalytic degradation process, facilitating the breakdown of malachite green into less harmful substances.

When determining the surface charge of the photocatalyst in relation to pH, a crucial consideration is the pH at the point of zero charge (pH_{zp}). The zeta potential, which indicates the surface charge of the photocatalyst, was measured at 5.12.

Overall, the zeta potential analysis confirms the suitability of the catalyst for practical applications in the removal of malachite green from contaminated water, highlighting its potential for environmental remediation.

The Mott-Schottky technique is a powerful method for investigating the electrical properties of semiconductor materials. By plotting the inverse square of the capacitance ($1/C^2$) against the applied voltage (V), valuable insights can be gained regarding the charge carrier concentration and the energy band structure of the semiconductor.

The BC/WO_3-CdS nanocomposite mentioned is characterized by its n-type conductivity, indicating that it is rich in electrons. The flat band potential of approximately 0.8 volts suggests the energy level at which the semiconductor's band structure aligns with the system's electrochemical potential (Fig. 6).

Photoluminescence (PL) spectroscopy is an effective method for evaluating the efficiency of electron-hole (e^-/h^+) pair separation in photocatalysts. The intensity of PL is inversely related to the rate at which charge carriers are separated; specifically, a lower PL intensity indicates a higher separation rate, which in turn enhances the efficiency of the photocatalyst.

As illustrated in Fig. 7, both WO_3 and the BC/WO_3-CdS nanocomposite exhibited significant PL quenching. This observation suggests that incorporating biochar and CdS effectively reduces the recombination of photogenerated electron-hole pairs. By minimizing this recombination, a greater number of charge carriers are available to engage in the photocatalytic reactions, ultimately improving the overall performance of the photocatalytic system.

3.3. *Effect of MG concentration*

The study investigated the photocatalytic degradation of MG at various initial concentrations ranging from 0.5 to 10 ppm. Table 1 displays the photocatalytic degradation efficiency of MG using BC/WO_3-CdS under visible light, revealing a decrease in efficiency as the concentration of MG increases. This decline can be attributed to the increased adsorption of MG molecules on the BC/WO_3-CdS surface at higher concentrations, resulting in a reduced number of available electron-hole pairs for photocatalysis. Furthermore, higher concentrations of MG lead to increased light absorption, which is essential for effective photocatalysis. Consequently, the overall photodegradation efficiency decreases. As a result, an optimal concentration of 2 ppm was selected.

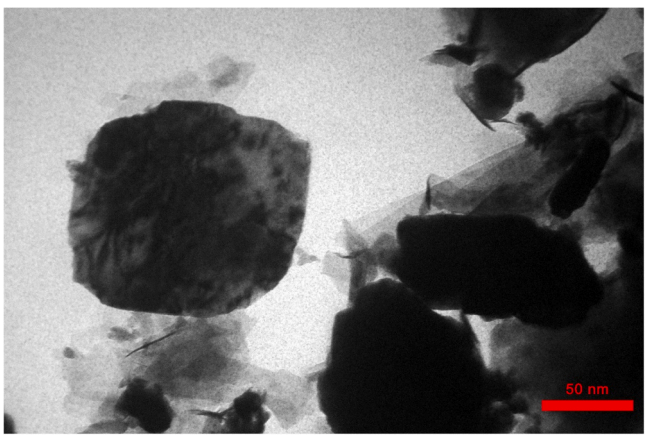

Fig. 4. TEM of BC/WO_3-CdS nanocomposite.

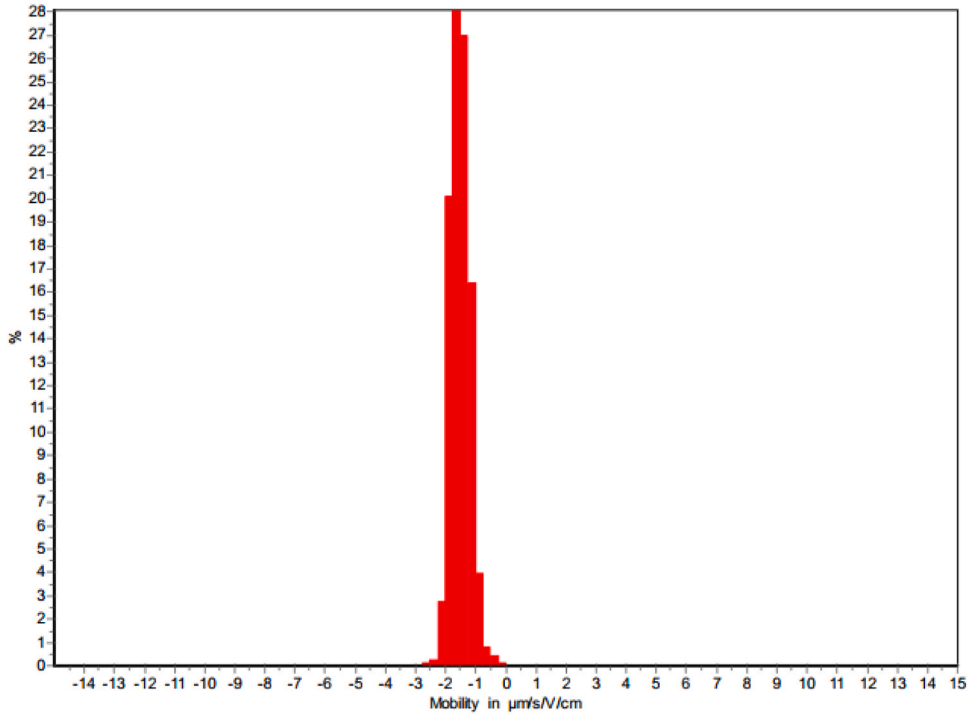

Fig. 5. Mobilities Distribution of BC/WO_3-CdS nanocomposite.

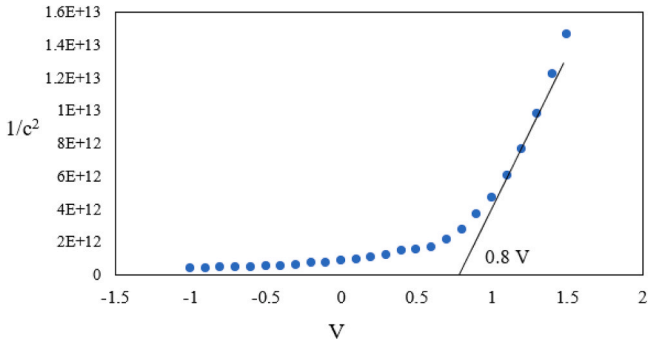

Fig. 6. Mott-Schottky curve of BC/WO_3-CdS nanocomposite.

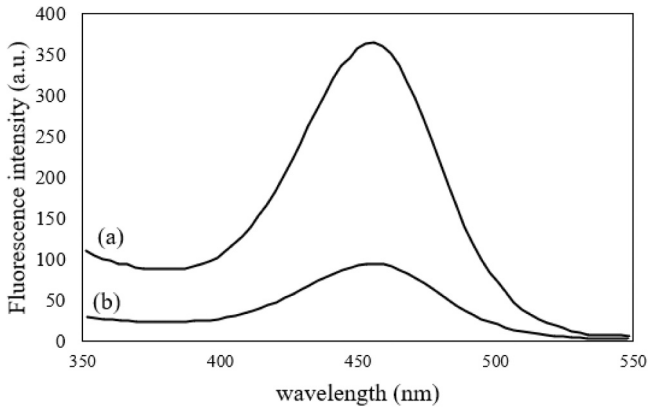

Fig. 7. PL emission spectra of (a) WO_3, and (b) BC/WO_3-CdS nanocomposite.

Table 1
Effect of the initial concentration of MG.

MG concentration (ppm)	Photocatalytic degradation (%)
0.5	98
1	97
2	97
4	96
6	92
8	89
10	86

3.4. Effect of catalyst amount on MG photodegradation

Different weight amounts of BC/WO_3-CdS heterogeneous photocatalysts were employed to assess their performance while maintaining a constant dye concentration of 2 ppm, as indicated in Table 2. The decomposition reaction demonstrates an increasing trend up to 200 mg of nanocatalyst in 10 mL of the dye solution. This can be attributed to the greater availability of reactive sites on the catalyst surface. However, beyond this point, the degradation process diminishes due to light scattering and reduced light penetration in the solution. The higher concentration of catalyst leads to the deactivation of activated molecules through collisions with lower energy molecules. Consequently, the turbidity of the medium increases, impeding light penetration and resulting in a decreased reaction rate. Additionally, the higher catalyst concentration limits light absorption and reduces the surface area due to nanocatalyst agglomeration.

3.5. Effect of pH on the MG photodegradation

The MG decomposition rate at different pH levels is depicted in Table 3. In an acidic environment, the presence of hydronium ions induces a positive charge, leading to a reduction in the number of active sites on the surface of the BC/WO_3-CdS heterogeneous catalyst. Consequently, the adsorption of cationic MG dye onto the catalyst surface becomes challenging due to the low concentration of active hydroxyl radicals. As a result, the decomposition of MG dye progresses slowly. However, as the pH increases, the decomposition rate also increases. This can be attributed to the primarily negative charge on the surfaces of the nanocatalyst, primarily due to the presence of hydroxyl groups. Higher pH values promote the formation of active •OH species, facilitating the transfer of holes to the adsorbed hydroxyls and promoting electrostatic attractive interactions between the negatively charged BC/WO_3-CdS heterogeneous catalyst particles and the cationic dyes present in the system. Based on our findings, we propose that the surface of BC/WO_3-CdS carries a negative charge, allowing the adsorption of MG dye onto it through the positively charged ammonium groups.

3.6. Photocatalytic reaction mechanisms

To evaluate the impact of active species generated by BC/WO_3-CdS on the photocatalytic degradation of MG, we investigated the removal percentage of this contaminant in the presence of various scavengers under optimal conditions. Fig. 8 illustrates the obtained results.

In this particular study, we employed different scavengers, namely isopropyl alcohol (IPA), 1,4-benzoquinone (BQ), and ammonium oxalate (AO), to quench •OH, $•O^{2-}$, and h^+ species, respectively, during the photocatalytic process. The extent of the decrease in the removal percentage of MG served as an indicator of the scavenger's impact.

As displayed in Fig. 8, the addition of IPA significantly reduced the MG removal efficiency from 97 % to 6.5 %, indicating the predominant role of •OH in the degradation process. Similarly, the presence of BQ led to a suppression in the degradation percentage, suggesting a slight involvement of $•O^{2-}$ in the degradation of MG. Conversely, the introduction of AO resulted in a marginal reduction in the removal efficiency, suggesting that h^+ species had minimal contribution to the degradation of MG within this photocatalytic system.

3.7. Kinetic analysis

The Langmuir-Hinshelwood equation (Eq. (2)) has commonly been employed to model the photocatalytic reaction kinetics of

Table 2
Effect of the amount of the photocatalyst.

Photocatalyst amount (mg)	Photocatalytic degradation (%)
50	85
100	91
200	97
300	90
400	73

Table 3
Effect of pH on MG photodegradation.

pH	Photocatalytic degradation (%)
4.0	77
6.0	91
8.0	98
10.0	83

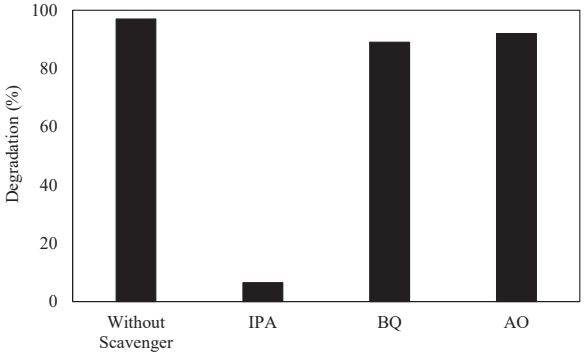

Fig. 8. Effect of scavengers on the photocatalytic degradation of MG.

various compounds (Mehrizad and Gharbani, 2017a, 2017b; Khosroshahi and Mehrizad, 2019; Qarajehdaghi et al., 2023; Abdarnezhadi and Mehrizad, 2023).

$$r = \frac{dC}{dt} = \frac{kKC}{1+KC} \tag{2}$$

Since KC is significantly smaller than 1, neglecting KC in the denominator and integrating over time t simplifies Eq. (1) to a pseudo-first-order kinetic equation (Eq. (3)).

$$\ln\frac{C_0}{C} = kKt = k_{app}t \tag{3}$$

The reaction rate is represented by r in this equation, the initial and final concentrations of the compound are indicated by C_0 and C, the irradiation time is indicated by t (min), the reaction rate constant is represented by k (min^{-1}), and the compound's adsorption coefficient on a photocatalyst particle is denoted by k.

The linear transformation $\ln (C_0/C) = k_{app}$ t. k_{app} (the apparent reaction rate constants) for the MG photocatalytic degradation were found by linear regression analysis of the experimental data (Fig. 9). The kinetic curves showing the MG degradation, as shown in Fig. 9, exhibit conformity with pseudo-first-order kinetics. The suggested kinetics for MG degradation within this procedure are confirmed by the correlation coefficient (R^2) values, which are more than 0.99.

As anticipated, increasing the light intensity significantly enhances the rate of MG degradation. With higher radiation intensity, a larger number of reactive species are generated in the solution, subsequently facilitating their interaction with and degradation of the

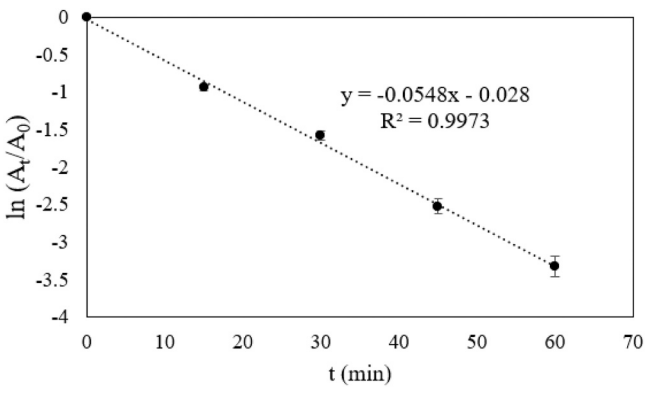

Fig. 9. ln A_t/A_0 versus visible irradiation time for MG degradation.

MG molecules.

3.8. Thermodynamic study

We employed the temperature-dependent fluctuation of k (303, 313, 323, and 333 K) to determine the activation energy (E_a) and other thermodynamic factors. The degradation's activation energy was calculated using the Arrhenius equation.

$$\ln k_{app} = - \frac{E_a}{RT} + \ln A \tag{4}$$

In this particular context, the symbol Kapp represents the apparent rate constant (min^{-1}), while A denotes the Arrhenius constant (min^{-1}). The universal gas constant is denoted by R (J mol^{-1} K^{-1}), and T represents the temperature in Kelvin. By plotting ln(k_{app}) against 1/T and analyzing the slope, the activation energy was determined, as depicted in Fig. 10a. The calculated activation energy was found to be 26.774 kJ mol^{-1}, indicating a moderate level. This suggests that the photocatalytic process has a relatively low barrier to entry. The Eqs. (5, and 6) were utilized to obtain the thermodynamic parameters based on the degradation test results at 298, 313, 323, and 333 K.

$$\ln \frac{k_{app}}{T} = \frac{-\Delta H^{\#}}{RT} + \ln \frac{k_B}{h} + \frac{\Delta S^{\#}}{R} \tag{5}$$

$$\Delta G = \Delta H - T\Delta S \tag{6}$$

Here, K_B is the Boltzmann constant. ΔH°, ΔS°, and ΔG° represent the enthalpy, entropy, and Gibbs free energy, respectively. Additionally, h denotes the Planck constant. To calculate the values of ΔH, ΔS, and ΔG, ln(k_{app}/T) was plotted against (1/T), as depicted in Fig. 10b. The resulting thermodynamic parameters are presented in Table 4. The negative ΔS° value (-0.186 KJ mol^{-1} K^{-1}) indicates a reduction in system unpredictability in the presence of degradation. Alternatively, due to the positive enthalpy values (24.19 kJ mol^{-1}), the degradation process of MG utilizing BC/WO_3-CdS photocatalyst is endothermic. The negative value of ΔG° suggests that the photocatalytic degradation process is non-spontaneous, requiring an input of energy to occur.

3.9. Comparison of BC/WO_3-CdS photocatalyst efficiency with other reports

The BC/WO_3-CdS nanocomposite was evaluated against previously reported photocatalysts for the degradation of methyl green. This evaluation was conducted based on several parameters, including irradiation time, apparent rate constant (K_{app}), and the percentage of degradation achieved. As illustrated in Table 5, the findings of the current study indicate that the proposed photocatalyst exhibits enhanced efficiency in the degradation of MG compared to those previously documented.

3.10. Effect of reusability of the BC/WO_3-CdS photocatalysts on MG degradation

The stability and reusability of a catalyst are essential factors to consider when designing a catalytic degradation process. In the case of BC/WO_3-CdS, its performance and durability were evaluated through multiple degradation cycles of MG. Fig. 11 provides a visual representation of these cycles. It shows that even after undergoing eight cycles, there is only a slight decrease in the photodegradation of the dye. This result indicates that the BC/WO_3-CdS nanocomposite exhibits a high level of stability and can maintain its catalytic activity over multiple uses. The good reusability of the catalyst is a favorable characteristic as it reduces the need for frequent replacement or regeneration, making the overall process more economically and environmentally sustainable. It also highlights the potential of BC/WO_3-CdS as a reliable and efficient catalyst for the photocatalytic degradation of MG. Further investigations and studies can be conducted to explore the long-term stability and reusability of BC/WO_3-CdS under various conditions, as well as its performance in degrading other contaminants. Such knowledge can contribute to optimizing its application in practical catalytic degradation processes and promoting its adoption in environmental remediation efforts.

4. Conclusion

The fabrication process of the BC/WO_3-CdS nanocomposite involved a simple technique that resulted in the successful synthesis of the desired material. The nanocomposite exhibited high crystallinity, indicating the formation of well-defined crystal structures within the material. When applied as a photocatalyst for the degradation of MG, the BC/WO_3-CdS nanocomposite displayed remarkable performance. After 60 minutes of exposure to visible light, a significant degradation rate of 98 % was achieved. This high degradation efficiency indicates the effectiveness of the nanocomposite in breaking down and removing the carcinogenic dye from the solution. The kinetics of the photocatalytic degradation process followed a pseudo-first-order model for MG. This implies that the degradation rate is directly proportional to the concentration of the pollutants, supporting the potential scalability and applicability of the BC/WO_3-CdS nanocomposite for the treatment of larger volumes of contaminated water. Overall, these findings emphasize the promising potential of the BC/WO_3-CdS nanocomposite as an efficient and reliable photocatalyst for the degradation of harmful and toxic pollutants, such as MG, in various aquatic environments. This research contributes to the development of sustainable and effective methods for water treatment and environmental remediation.

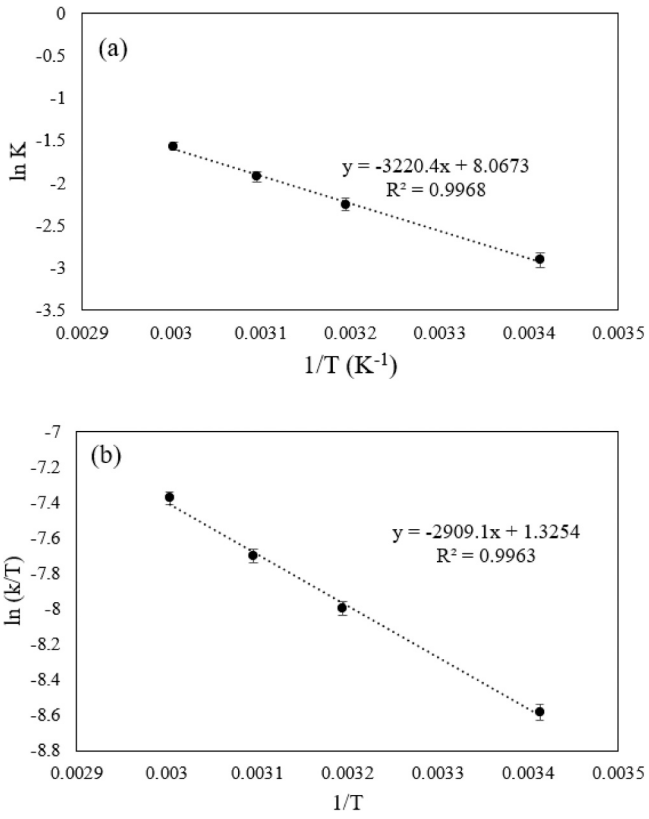

Fig. 10. The plots of ln k_{app} vs. 1/T (a), and ln (k_{app}/T) vs. 1/T (b) for the MG degradation using the BC/WO_3-CdS photocatalyst.

Table 4
The thermodynamic parameters for MG degradation using the BC/WO_3-CdS photocatalyst.

Temperature (k)	k_{app}	E_a (KJ/mol)	$\Delta H^{\#}$ (KJ/mol)	$\Delta G^{\#}$ (KJ/mol)	$\Delta S^{\#}$ (KJ/molK)
298	0.0548	26.774	24.19	79.62	−0.186
313	0.1052			82.41	
323	0.1456			84.27	
333	0.208			86.13	

Table 5
Comparison of photodegradation of MG using different catalyst.

Catalyst	Time (min)	K_{app} (min^{-1})	Degradation (%)	Ref
g-C_3N_4/Bi_2S_3/$NiFe_2O_4$	58	0.0504	95.6	(Merci et al., 2025)
$ZnFe_2O_4$/CeO_2	180	0.0035	96	(Raja et al., 2019)
Cu/ZnO nanoparticles	-	0.01	23.6	(Modwi et al., 2017)
ZnO NPs	120	0.02	92	(Meena et al., 2022)
BC/WO_3-CdS	60	0.0548	98	This work

Research ethics

No Research Ethics were received for this work.

Author agreement statement

We the undersigned declare that this manuscript is original, has not been published before and is not currently being considered for publication elsewhere.

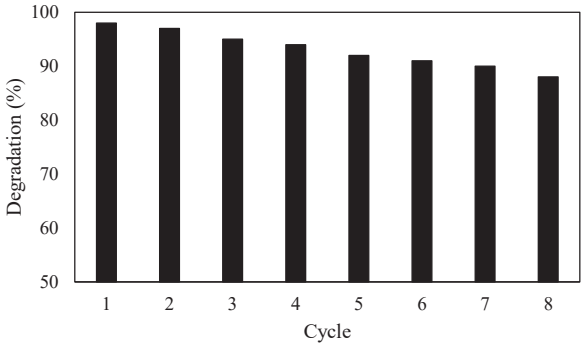

Fig. 11. Recycling runs of BC/WO_3-CdS for degradation of MG.

We confirm that the manuscript has been read and approved by all named authors and that there are no other persons who satisfied the criteria for authorship but are not listed. We further confirm that the order of authors listed in the manuscript has been approved by all of us.

We understand that the Corresponding Author is the sole contact for the Editorial process. He/she is responsible for communicating with the other authors about progress, submissions of revisions and final approval of proofs Signed by all authors as follows:

Intellectual property

We confirm that we have given due consideration to the protection of intellectual property associated with this work and that there are no impediments to publication, including the timing of publication, with respect to intellectual property. In so doing we confirm that we have followed the regulations of our institutions concerning intellectual property.

Funding

No funding was received for this work.

CRediT authorship contribution statement

Abolghasemi Mahani Amin: Writing – review & editing, Supervision, Investigation. **Salimi Mahdi:** Writing – original draft, Methodology, Formal analysis.

Declaration of Competing Interest

No conflict of interest exists. We wish to confirm that there are no known conflicts of interest associated with this publication and there has been no significant financial support for this work that could have influenced its outcome.

Data availability

The data that has been used is confidential.

References

Abdarnezhadi, R., Mehrizad, A., 2023. Flowerlike Sm–ZnIn2S4 as a susceptible visible-light photocatalyst for Cr6+ reduction: experimental design, RSM, and ANN modeling. J. Inorg. Organomet. Polym. Mater. 33 (6), 1621–1637.

Ali, I., Burakova, I., Galunin, E., Burakov, A., Mkrtchyan, E., Melezhik, A., Kurnosov, D., Tkachev, A., Grachev, V., 2019. High-speed and high-capacity removal of methyl orange and malachite green in water using newly developed mesoporous carbon: kinetic and isotherm studies. ACS Omega 4 (21), 19293–19306.

Arai, T., Horiguchi, M., Yanagida, M., Gunji, T., Sugihara, H., Sayama, K., 2009. Reaction mechanism and activity of WO3-catalyzed photodegradation of organic substances promoted by a CuO cocatalyst. J. Phys. Chem. C. 113 (16), 6602–6609.

Awad, A.M., Jalab, R., Benamor, A., Nasser, M.S., Ba-Abbad, M.M., El-Naas, M., Mohammad, A.W., 2020. Adsorption of organic pollutants by nanomaterial-based adsorbents: an overview. J. Mol. Liq. 301, 112335.

Bao, N., Shen, L., Takata, T., Domen, K., 2008. Self-templated synthesis of nanoporous CdS nanostructures for highly efficient photocatalytic hydrogen production under visible light. Chem. Mater. 20 (1), 110–117.

Berberidou, C.P., Poulios, I., Xekoukoulotakis, N.P., Mantzavinos, D., 2007. Sonolytic, photocatalytic and sonophotocatalytic degradation of malachite green in aqueous solutions. Appl. Catal. B: Environ. 74 (1-2), 63–72.

Bulgariu, L., Escudero, L.B., Bello, O.S., Iqbal, M., Nisar, J., Adegoke, K.A., Alakhras, F., Kornaros, M., Anastopoulos, I., 2019. The utilization of leaf-based adsorbents for dyes removal: a review. J. Mol. Liq. 276, 728–747.

Cai, Y., Luo, Y., Xiao, Y., Zhao, X., Liang, Y., Hu, H., Dong, H., Sun, L., Liu, Y., Zheng, M., 2016. Facile synthesis of three-dimensional heteroatom-doped and hierarchical egg-box-like carbons derived from Moringa oleifera branches for high-performance supercapacitors. ACS Appl. Mater. Interfaces 8 (48), 33060–33071.

Deng, C., Tian, X., 2013. Facile microwave-assisted aqueous synthesis of CdS nanocrystals with their photocatalytic activities under visible lighting. Mater. Res. Bull. 48 (10), 4344–4350.
Gupta, V.K., Jain, R., Nayak, A., Agarwal, S., Shrivastava, M., 2011. Removal of the hazardous dye—Tartrazine by photodegradation on titanium dioxide surface. Mater. Sci. Eng.: C. 31 (5), 1062–1067.
Huang, C., Sun, T., Hulicova-Jurcakova, D., 2013. Wide electrochemical window of supercapacitors from coffee bean-derived phosphorus-rich carbons. ChemSusChem 6 (12), 2330–2339.
Kang DongJuan K.D., Yu XiaoLin Y.X., Ge MaoFa G.M., Xiao Feng X.F., Xu Hui X.H. (n.d) Novel Al-doped carbon nanotubes with adsorption and coagulation promotion for organic pollutant removal.
Katheresan, V., Kansedo, J., Lau, S.Y., 2018. Efficiency of various recent wastewater dye removal methods: A review. J. Environ. Chem. Eng. 6 (4), 4676–4697.
Khosroshahi, A.G., Mehrizad, A., 2019. Optimization, kinetics and thermodynamics of photocatalytic degradation of Acid Red 1 by Sm-doped CdS under visible light. J. Mol. Liq. 275, 629–637.
Kim, Y.H., Irie, H., Hashimoto, K., 2008. A visible light-sensitive tungsten carbide/tungsten trioxde composite photocatalyst. Appl. Phys. Lett. 92 (18).
Liu, X., Sayed, M., Bie, C., Cheng, B., Hu, B., Yu, J., Zhang, L., 2021. Hollow CdS-based photocatalysts. J. Mater. 7 (3), 419–439.
Mashkoor, F., Nasar, A., 2020. Magsorbents: Potential candidates in wastewater treatment technology–a review on the removal of methylene blue dye. J. Magn. Magn. Mater. 500, 166408.
Meena, P.L., Poswal, K., Surela, A.K., 2022. Facile synthesis of ZnO nanoparticles for the effective photodegradation of malachite green dye in aqueous solution. Water Environ. J. 36 (3), 513–524.
Mehrizad, A., Gharbani, P., 2017b. Synthesis of ZnS decorated carbon fibers nanocomposite and its application in photocatalytic removal of Rhodamine 6G from aqueous solutions. Prog. Color., Color. Coat. 10 (1), 13–21.
Mehrizad, A., Gharbani, P., 2017a. Optimization of operational variables and kinetic modeling for photocatalytic removal of direct blue 14 from aqueous media by ZnS nanoparticles. J. Water Health 15 (6), 955–965.
Merci, S., Shamspur, T., Mostafavi, A., 2025. Synthesis of a direct dual Z-scheme g-C3N4/Bi2S3/NiFe2O4 photocatalyst for degradation of organic pollutants: optimization using response surface methodology. Appl. Organomet. Chem. 39 (1), e7883.
Miyauchi, M., 2008b. Photocatalysis and photoinduced hydrophilicity of WO 3 thin films with underlying Pt nanoparticles. Phys. Chem. Chem. Phys. 10 (41), 6258–6265.
Miyauchi, M., 2008a. Photocatalysis and photoinduced hydrophilicity of WO 3 thin films with underlying Pt nanoparticles. Phys. Chem. Chem. Phys. 10 (41), 6258–6265.
Modwi, A., Abbo, M.A., Hassan, E.A., Al-Duaij, O.K., Houas, A., 2017. Adsorption kinetics and photocatalytic degradation of malachite green (MG) via Cu/ZnO nanocomposites. J. Environ. Chem. Eng. 5 (6), 5954–5960.
Qarajehdaghi, M., Mehrizad, A., Gharbani, P., Shahverdizadeh, G.H., 2023. Quaternary composite of CdS/g-C3N4/rGO/CMC as a susceptible visible-light photocatalyst for effective abatement of ciprofloxacin: Optimization and modeling of the process by RSM and ANN. Process Saf. Environ. Prot. 169, 352–362.
Qu, W.H., Xu, Y.Y., Lu, A.H., Zhang, X.Q., Li, W.C., 2015. Converting biowaste corncob residue into high value added porous carbon for supercapacitor electrodes. Bioresour. Technol. 189, 285–291.
Raja, V.R., Karthika, A., Kirubahar, S.L., Suganthi, A., Rajarajan, M., 2019. Sonochemical synthesis of novel ZnFe2O4/CeO2 heterojunction with highly enhanced visible light photocatalytic activity. Solid State Ion. 332, 55–62.
Salavati-Niasari, M., Davar, F., Loghman-Estarki, M.R., 2009. Long chain polymer assisted synthesis of flower-like cadmium sulfide nanorods via hydrothermal process. J. Alloy. Compd. 481 (1-2), 776–780.
Saleh, T.A., Gupta, V.K., 2014. Processing methods, characteristics and adsorption behavior of tire derived carbons: a review. Adv. Colloid Interface Sci. 211, 93–101.
Sanghi, R., Verma, P., 2009. A facile green extracellular biosynthesis of CdS nanoparticles by immobilized fungus. Chem. Eng. J. 155 (3), 886–891.
Singh, N.B., Nagpal, G., Agrawal, S., 2018. Water purification by using adsorbents: a review. Environ. Technol. Innov. 11, 187–240.
Torimoto, T., Nakamura, N., Ikeda, S., Ohtani, B., 2002. Discrimination of the active crystalline phases in anatase–rutile mixed titanium (IV) oxide photocatalysts through action spectrum analyses. Phys. Chem. Chem. Phys. 4 (23), 5910–5914.
Wong, S., Ngadi, N., Inuwa, I.M., Hassan, O., 2018. Recent advances in applications of activated carbon from biowaste for wastewater treatment: a short review. J. Clean. Prod. 175, 361–375.
Xu, D., Tong, Y., Yan, T., Shi, L., Zhang, D.N., 2017. P-codoped meso-/microporous carbon derived from biomass materials via a dual-activation strategy as high-performance electrodes for deionization capacitors. ACS Sustain. Chem. Eng. 5 (7), 5810–5819.
Yang, F., Zhang, S., Sun, Y., Cheng, K., Li, J., Tsang, D.C., 2018. Fabrication and characterization of hydrophilic corn stalk biochar-supported nanoscale zero-valent iron composites for efficient metal removal. Bioresour. Technol. 265, 490–497.
Zhang, Y.C., Wang, G.Y., Hu, X.Y., 2007. Solvothermal synthesis of hexagonal CdS nanostructures from a single-source molecular precursor. J. Alloy. Compd. 437 (1-2), 47–52.
Zhao, R., Li, Y., Sun, B., Chao, S., Li, X., Wang, C., Zhu, G., 2019. Highly flexible magnesium silicate nanofibrous membranes for effective removal of methylene blue from aqueous solution. Chem. Eng. J. 359, 1603–1616.
Zhao, Z.G., Miyauchi, M., 2008. Nanoporous-walled tungsten oxide nanotubes as highly active visible-light-driven photocatalysts. Angew. Chem. Int. Ed. 47 (37), 7051–7055.
Zhou, Y., Lu, J., Zhou, Y., Liu, Y., 2019. Recent advances for dyes removal using novel adsorbents: a review. Environ. Pollut. 252, 352–365.
Zhu, H., Wang, X., Yang, F., Yang, X., 2011. Promising carbons for supercapacitors derived from fungi. Adv. Mater. 24 (23), 2745–2748.